GEOGRID PULLOUT BEHAVIOUR ACCORDING TO THE EXPERIMENTAL EVALUATION OF THE ACTIVE LENGTH

G. Cardile[1], N. Moraci[2] and L.S. Calvarano[3]

1 Assistant Professor of Geotechnical Engineering, Ph.D. — *Mediterranea* University of Reggio Calabria, Department of Civil Engineering, Energy, Environment and Materials (DICEAM), Italy- Telephone: +39 0965 169 2213; Telefax: +39 0965 1692201, e-mail: giuseppe.cardile@unirc.it

2 Full Professor of Geotechnical Engineering, Ph.D. — *Mediterranea* University of Reggio Calabria, Department of Civil Engineering, Energy, Environment and Materials (DICEAM), Italy- Telephone: +39 0965 169 2263; Telefax: +39 0965 1692201, e-mail: nicola.moraci@unirc.it

3 Research assistant in Geotechnical Engineer, Ph.D. — *Mediterranea* University of Reggio Calabria, Department of Civil Engineering, Energy, Environment and Materials (DICEAM), Italy- Telephone: +39 0965 169 2306; Telefax: +39 0965 1692201, e-mail: lidia.calvarano@unirc.it

ABSTRACT

In reinforced earth structures, the main function of the included reinforcement is to redistribute stresses within the soil mass in order to enhance internal stability. Redistribution of internal stresses in reinforced soil can be very complex. In order to simulate the behaviour of geosynthetic reinforcement, large-scale laboratory pullout tests are carried out. Once a pullout load has been applied, the tensile force is transferred along the geogrid (from the front to the free end) and reduced through interaction with the soil. The active length is the portion of the geogrid on which the mobilization of interaction mechanisms withstands the applied pullout load. Evaluation of the active length can allow for the understanding of the interaction mechanisms and can therefore be important for the design of the soil-geosynthetic interface.

This paper describes the interpretation of pullout test results based on an experimental and theoretical evaluation of the active length. This approach has been used to analyse several large-scale pullout tests performed on two extruded geogrids embedded in a compacted granular soil, varying the specimen lengths and the applied effective vertical pressures.

1 INTRODUCTION

Knowledge of the mechanical behaviour of the soil-geosynthetic interface under pullout conditions is important to analyse the behaviour of reinforced earth structures. Large scale pullout tests permit the study of interaction between soil and geosynthetics in the anchorage zone and determination of the parameters of soil-geosynthetic interaction for the design of reinforced soil structures. Test results can be used: (i) to derive the constitutive model for the soil–geosynthetic interface, which is necessary to FEM analysis, (ii) to obtain the interface apparent coefficient of friction, which is necessary in the limit equilibrium analysis.

When a pullout load is applied, the tensile force is transferred from the front to the free end of the geogrid. Figure 1 shows a scheme of this pullout load transfer mechanism. For extensible geosynthetic reinforcements under pullout loading conditions, considerable elongation of the longitudinal ribs of the geogrid occur. Therefore, under an applied pullout force and confining vertical effective pressure, only a frontal portion of the geogrid displaces relative to the surrounding soil. The distribution of internal tensile stresses (which defines the shapes of the distribution curve) can be very complex, depending on: (i) boundary conditions, (ii) mechanical properties of the soil, and (iii) structural, geometrical and mechanical characteristics of the geosynthetic reinforcement (Laba *et al.* 1984; Ochiai *et al.* 1992; Abramento and Whittle 1995; Alagiyawanna *et al.* 2001; Sugimoto *et al.* 2001; Moraci and Cardile 2009; Moraci *et al.* 2009; Cazzuffi *et al.* 2011; Moraci and Cardile 2012; Zhou *et al.* 2012; Vieira *et al.* 2013; Calvarano *et al.* 2014; Cardile *et al.* 2014; Cazzuffi *et al.* 2014a; Cazzuffi *et al.* 2014b; Moraci *et al.* 2014a; Moraci *et al.* 2014b).

The main interaction mechanisms affecting the pullout resistance of geogrids are the skin friction, between soil and reinforcement solid surface, and the bearing resistance which is developed against transversal elements (Ziegler and Timmers 2004; Moraci and Gioffrè 2006; Moraci *et al.* 2007; Palmeira 2009; Jacobs *et al.* 2014; Moraci *et al.* 2014a). The active length is the portion of the geogrid specimen on which the mobilization of interaction mechanisms withstands the applied load. Furthermore determining the active length is important to understand the actual behaviour of the soil-geosynthetic interface during the two phases of the process: (i) load transfer and (ii) pullout (Moraci and Recalcati 2006; Moraci and Cardile 2008).

Recently, different researchers analysed the behaviour at the interface using micro-image analysis system (Zhou *et al.* 2012; Ezzein and Bathurst 2014; Bathurst and Ezzein 2015).

Zhou et al. (2012) clarify the interaction mechanism between sand and geogrid transversal ribs showing that sand particles in front of the transverse rib rotate during pullout. Particles above the reinforcement symmetry axis rotate clockwise, while particles below the symmetry axis rotate counterclockwise. Particles on the top-right side of transverse rib fall into the voids created during the geogrid movement. The micro-image analysis confirms the macroscopic observations that the soil in front of transverse rib is subjected to a passive state of stress, while an active stress-state is reached behind it, creating loose soil regions. Additionally, it is worth noting that due to the different boundary conditions sand particles do not move symmetrically along the interface (Moraci *et al.* 2014a) .

Bathurst and Ezzein (2015) measured the complete displacement field of reinforcement and target particles seeded in the surrounding soil during pullout tests by using a novel combination of technologies (transparent granular soil and DIC/PIV technique of digital image processing). Technologies, which are useful to analyse the relative horizontal displacement between the geogrids and surrounding soil.

This paper describes the interpretation of several large-scale pullout tests performed on two extruded geogrids embedded in a compacted granular soil based on an experimental and theoretical evaluation of the active length.

2 PULLOUT EQUIPMENT

Test apparatus used in this research work is the same already presented in a previous study (Moraci and Recalcati 2006). The apparatus is essentially composed of: (i) a large, steel pullout box (1700x600x680 mm), (ii) an airbag (an air-filled cushion) used to apply the vertical load, (iii) an electric jack actuator used to apply the horizontal pullout force, which is measured using a load cell, and (iv) all the required control and data-acquisition instruments. Displacements of transverse ribs of geogrid specimen are recorded using inextensible steel wires (or steel rods) connected to rotary variable displacement transducers (RVDT), which are connected to the external backside of the box (Figure 2).

Using this apparatus, it is also possible to study the confined failure of the geosynthetic specimen by using a clamp placed inside the soil, kept well away from the frontal wall by using metal sleeves in order to maintain the specimen in a confined condition for the duration of the test. To overcome issues related

to friction between the metal clamp and the metal sleeves, preliminary pullout tests were conducted on the clamp alone, under the same confining pressure used in the geogrid tests. It was accurately checked that no relative displacement between clamp and geogrids occurred.

The main factors affecting the results of the pullout test are: (i) test apparatus and test procedure, (ii) the geotechnical properties of the soil, and (iii) the characteristics of the reinforcement. The pullout device and procedure used in this research takes into account box dimensions and methods in order to minimize the effects of boundary conditions on the test results (Moraci *et al.* 2014a).

Multiple pullout tests were performed varying specimen length (L_R) and applied vertical effective pressure (σ'_v). All tests were performed at controlled rates of displacement equal to 1.0 mm/min until either the geogrid ruptured or total horizontal displacement reached 100 mm.

3 TEST MATERIALS

Two extruded, mono-directional, High-Density Polyethylene (HDPE) geogrids (GGR1 and GGR2), were used for the pullout tests.

Due to the viscous-elastic-plastic properties of their constituent polymer, mechanical properties of geogrids depend on test temperature and test rate (Kongkitkul *et al.* 2014). Therefore, the mechanical characteristics of these geosynthetics were evaluated by means of in-isolation, wide-width tensile tests (UNI EN ISO 10319:2008) performed at displacement rates of 1 mm/min (the same test rate used in the pullout tests) and under controlled temperature. The tensile test results at a displacement rate of 1 mm/min and the main geometrical properties of the geogrids are reported in *Table* 1.

The soil used in these tests, Figure 3, was classified as uniform, medium sand (SP according to USCS classification system; A-3 according to CNR-UNI 10006 classification system), with grain shape ranging from sub-rounded to rounded, uniformity coefficient ($U = D_{60}/D_{10}$) equal to 1.96, and average grain size (D_{50}) equal to 0.32 mm.

Standard Proctor compaction tests gave a maximum dry unit weight $\gamma_{dmax} = 16.24$ kN/m^3 at an optimum water content $w_{opt} = 13.5\%$.

Direct shear tests, performed at 95% of γ_{dmax}, yielded values of the peak shear-strength angle ϕ'_P from 48° (for σ'_v =10 kPa) to 42° (for σ'_v =100 kPa). The shear-strength angle at constant volume ϕ'_{CV} was equal to 34° (Moraci and Recalcati 2006).

4 ANALYSIS OF TEST RESULTS

4.1 Pullout load transfer mechanism

Pullout tests have been performed varying the specimen length (L_R = 0.40, 0.90, 1.15 m) while keeping the specimen width constant (W = 0.58 m). Applied vertical effective pressures were equal to 10, 25, 50 and 100 kPa. The displacement rate was 1.0 mm/min in all tests. Therefore, 24 different pullout test combinations were studied.

In order to explain the pullout load transfer mechanism it is possible to use the results of any pullout test. For instance, the curves in Figure 4 represent the distributions of the nodal (transversal rib) displacements along the geogrid specimen (in this case, GGR2) for different values of applied pullout force (at σ'_v=50 kPa). The slope of each curve represents the local strain (Moraci and Recalcati 2006). The upper and lower graphs refer to short and long reinforcements, respectively. The graphs in Figure 4a show the *tensile load transfer phase*. During this phase, active length increases with pullout force until a limit value (trigger force P_{in}), at which movement of the last rib is observed (the dotted line refers to this trigger force). By contrast, the graphs in Figure 4b refer to the *pullout phase*. Once two adjacent curves are parallel to each other, as in the case of ‘‘short’’ reinforcement, pullout occurs.

Due to the effect of reinforcement extensibility there are relevant differences in the mobilization of interface mechanisms. Generally, for ‘‘long’’ reinforcement or relatively low reinforcement stiffness (and, generally, for high values of confining pressure), a progressive mobilization of the mechanisms of interface interaction develops; this is highlighted by the non-linearity of the nodal displacement distribution. On the other hand, for short reinforcement or high reinforcement stiffness (and, generally, at low values of σ'_v), these mechanisms are activated almost at the same time along the whole reinforcement.

Therefore, due to this extensibility effect, the distribution of the displacement and therefore of shear stress is non-uniform along the length of an inclusion.

4.2 Experimental evaluation of the active length

The displacement of the transversal ribs during the pullout tests was measured using inextensible steel wires connected to displacement transducers (RVDT) connected to the external backside of the box. Once a rib's displacement has been recorded, the active length is equal to the specimen portion (inclusive of its elongation) from the clamp (first section of the confined specimen) to the mobilized rib. The experimental values of the active length, L_A, measured with increasing pullout load, P, are plotted in Figure 5, referring to pullout tests performed on GGR2 under a confining pressure of 50 kPa.

The experimental points recorded for each transversal rib, at the same vertical confining pressure and varying the specimen length, have been interpolated using the following best-fitting logarithmical function:

$$P = a \cdot [\ln(b \cdot L_A) + 1] \quad (1)$$

where the coefficients *a* and *b* are experimental parameters obtained through data fitting. The coefficients depend on the mechanical parameters of the soil, the applied confining pressure and the geometrical and mechanical characteristics of the geogrid.

Until the pullout phase starts (when the free end of the geogrid begins to move), the pullout behaviour of the mechanical interface is not affected by the total length of the embedded reinforcement, depending for the same geogrid only on the confining vertical pressure.

Figure 6 shows the different active length curves obtained for all the investigated geogrids and confining vertical pressures. In each graph, for the same geogrid and compacted-soil fill, the logarithmic best-fitting trends related to different applied confining pressures are plotted along with the experimental results. It is clear that the experimental results are in good agreement with the proposed logarithmic best-fitting function.

4.3 Longitudinal strain

In order to take into account that, under pullout load conditions, load and elongation act on a reinforcement portion that varies during the duration of the tests (i.e., the active length), it is possible to define average longitudinal strain ε_A as the ratio between the recorded total elongation of the specimen ΔL and the related active length L_A minus ΔL:

$$\varepsilon_A = \Delta L / \left(L_A - \Delta L \right) \quad (2)$$

The confined portions along the geogrid specimen (respectively labelled: 0-1, 1-2, 2-3, 3-4, 4-5, see Figure 2) were monitored during the tests.

In Figure 7, the pullout loads are plotted versus the strains on these portions for each geogrid specimen (GGR1 in Figure 7a and GGR2 in Figure 7b) of length L_R = 1.15 m and under an applied confining pressure of 50 kPa. The highest average longitudinal strain among those of the different investigated portions was measured for the portion closest to the clamp. Particularly, the average longitudinal strain on the portion nearest to the clamp is very large compared to the corresponding value calculated on the active length (portion 0-L_A, the solid line in Figure 7). The pullout stiffness of the initial portion is lower than the value obtained by in-isolation wide-width tensile tests (performed at v = 1 mm/min, see *Table* 1), probably because the average rate of displacement in the pullout test along the geogrid specimen and during the transfer phase is lower than 1 mm/min.

During the tensile load transfer phase of the pullout load, the average longitudinal strain calculated on the active length portion 0-L_A is an increasing function of the vertical confining pressure (Figure 8). For the same pullout load, higher average strains were obtained for the geogrid GGR2. This results depends on the different geogrid stiffness (GGR1 is stiffer than GGR2) and on the different geometry of the transversal ribs of the two geogrids (GGR2 has less passive surface than GGR1). According to Moraci and Gioffrè (2006), the passive surface is the surface of each rib element (including the single node and the bar portion between two nodes) where the bearing resistance can be mobilized.

In the upper graph of Figure 9, the active length is plotted versus the clamp displacement (displacement of the first confined section) of GGR2. This result refers to pullout tests performed on geogrid GGR2 for fixed values of confined pressure (50 kPa) and specimen length (1.15 m). In the bottom part of the

figure, the displacements are related to the average longitudinal strain. The marker in this figure shows the beginning of the pullout phase, which separates the two phases (tensile load transfer phase and pullout phase). In the pullout phase, increasing active length is only due to elongation of the geogrid. Figure 10 shows all the pullout test results performed on GGR2 at the same confining pressure but with different specimen lengths according to this approach. The gradient of the average longitudinal strain recorded in the tensile load transfer phase is smaller than that recorded during the pullout phase. Once the average longitudinal strain has stopped increasing (in other words, when the curves that show nodal displacement along the specimen are parallel to each other), pullout failure occurs (according to Moraci and Recalcati (2006) pullout failure occurs when the top curves in Figures 4 are parallel to each other, as in case of reinforcement with L_R = 0.40 m at $\delta \approx 40$ mm in Figure 10).

Table 2 shows that the values of average longitudinal strain calculated at the beginning of the pullout phase ε_{AP} (for each specimen length) increase with increasing confining pressure for both investigated geogrids.

4.4 Average shear stress

Pullout test results for the investigated extensible geogrid inclusions have shown that displacement and the strain along the reinforcement's length do not vary linearly (Perkins and Cuelho 1999; Moraci and Recalcati 2006; Wang *et al.* 2014). Therefore, the shear stress along the interface between the soil and the geogrid reinforcement is not uniform. The actual value of the shear stress along the interface depends on the reinforcement's confined stiffness (extensibility) and on the developed shear stresses along the active interface of the geogrid.

In this paper, in order to simplify the experimental interpretation, the actual shear stress that is mobilized along the interface between the active length of the geogrid and the surrounding soil is replaced by an equivalent, uniform, average shear-stress distribution τ_{AL} (Figure 11). The ratio between the applied pullout load (P) and the double active length (L_A) obtains the average shear stress:

$$\tau_{AL} = \frac{P}{2 \cdot L_A} \tag{3}$$

Figure 12 shows the average shear stress versus clamp displacement, calculated using equation (3), for geogrid GGR2 of fixed specimen length (L_R = 1.15 m) and varying the confining pressure. As expected, average shear stress increases with increasing vertical effective pressure. The large marks on the graph show when the pullout phase starts.

Figure 13 shows the pullout behaviour in terms of average shear stress of GGR2 for a fixed vertical effective pressure (50 kPa) and varying the specimen lengths. It is obvious that until the active length is shorter than the geogrid specimen length, the experimental results are the same.

During the *tensile load transfer phase*, average shear stress decreases with increasing displacement of the first confined geogrid section, despite a local increase in frictional and passive stresses along the geogrid. The growing pullout force is mobilized, in this phase, on an active length that increases very rapidly.

When the *pullout phase* starts, the active length becomes almost constant ($L_R+\Delta L$), while the pullout load continues to grow. Therefore, the trend in average shear stress changes, as it increases with increasing displacement.

Once the pullout phase starts, the interaction mechanisms in the short specimen (low extensibility) are mobilized almost immediately and simultaneously along the active length. The progressive failure mechanisms related to the long reinforcement (high extensibility) produces a lower peak of apparent shear stress mobilized at higher displacements. Once longitudinal strain stops increasing, pullout occurs and average shear stress rapidly decreases.

4.5 Apparent coefficient of friction of the soil–geosynthetic interface

Analysis of pullout test results leads to an apparent coefficient of friction of the soil–geosynthetic interface, defined as:

$$\mu_{S/GSY}^{AL} = \frac{P}{2 \cdot L_A \cdot \sigma'_V} \qquad (4)$$

The calculated apparent coefficients of friction are shown in Figure 14 for the geogrid GGR2 under two different vertical effective pressures (50 and 100 kPa in Figures 14a and 14b, respectively) and varying

242 the reinforcement length. In each graph, the apparent coefficient of friction of the soil-geosynthetic
243 interface is plotted versus the clamp displacement.
244 The curves plotted with the different symbols refer to the apparent coefficient of friction at the interface
245 calculated using the active length ($\mu_{S/GSY}^{AL}$), while the dashed curves refer to friction coefficients
246 calculated using the total specimen length ($\mu_{S/GSY}$).
247 The pullout behaviour in the two phases is similar to that previously described for the apparent effective
248 shear stresses. For small displacements, once the overall specimen length has been mobilized, the values
249 of the actual apparent coefficient of friction are higher than those calculated by using the specimen
250 length (the dashed curves).
251 These graphs could be used in order to evaluate, for different specimen lengths, the design value of the
252 apparent coefficient of friction of the soil-geosynthetic interface related to the admissible displacement
253 of reinforcement mobilized in the *tensile force transfer phase*.
254

255 **4.6 Apparent pullout stiffness**

256 The apparent pullout stiffness is defined as the ratio between the applied pullout load and the related
257 average longitudinal strain (mobilized on the active length):

258 $$J_a^{\sec} = \frac{P}{\varepsilon_a} \qquad (5)$$

259 Therefore, in the paper, the stiffness value able to predict, for the applied pullout load, the integrated
260 response along the active length of soil reinforcement interaction was defined as apparent confined
261 stiffness. It is important to emphasise that, using this definition, the ε_a evaluated along the L_A implicitly
262 takes into account soil-geosynthetic interaction.
263 In Figure 15, the apparent pullout stiffness is plotted versus average longitudinal strain; these results
264 were obtained by pullout tests performed on GGR1 (Figure 15a) and GGR2 (Figure 15b) geogrid
265 specimens, varying the specimen length and under the same vertical effective pressure (50 kPa). During
266 the *tensile load transfer phase*, apparent pullout stiffness rapidly increases with increasing average
267 longitudinal strain, which has very small values (1-2% for GGR1; 2-3% for GGR2). Under the same

vertical effective pressure, the short reinforcements show a lower maximum value for apparent pullout stiffness than the values evaluated for the long specimens. Until the whole specimen length is mobilized (in the *tensile load transfer phase*), pullout resistance increases with small increases in average strain; when the *pullout phase* begins, apparent pullout stiffness decreases with increasing strain. When pullout failure occurs (i.e., in the short reinforcement curve in Figure 15), a sudden decrease in apparent pullout stiffness is observed.

Figure 16 shows the influence of vertical effective pressure on the apparent pullout stiffness of GGR1 (Figure 16a) and GGR2 (Figure 16b) geogrid specimens for the same length (L_R = 1.15 m). The peak value of apparent pullout stiffness decreases with increasing vertical effective pressure (from 2936 to 1706 kN/m for GGR1 and from 1363 to 985 kN/m for GGR2). Moreover, the peak value is mobilized for an average strain that increases with increasing vertical effective pressure (from 0.6 to 3.6% for GGR1 and from 1.2 to 4.4% for GGR2).

Comparing the pullout test results with the in-isolation wide-width tensile test, notice that during the pullout phase, apparent longitudinal confined stiffness decreases with increasing average longitudinal strain until reaching the in-air tensile stiffness (for the same level of strain).

The results of pullout tests performed on geogrid specimens of L_R= 1.15 m are summarized in Table 3 and *Table 4*, showing that peak values of the apparent pullout stiffness (defined in equation (5)) are greater than tensile stiffness obtained by in-isolation wide-width tensile tests for the same level of strain (the differences range from 22 to 50%), as shown in Figure 17. These results depend on the fact that, under confined conditions, due to interface interaction mechanisms, the tensile load varies along the specimen (contrary to the unconfined case).

Stability analysis performed by means of the equilibrium limit method (the most common approach for analysing the stability of reinforced slopes) does not consider serviceability requirements. If safety factors satisfy typical design criteria, the displacement will likely be within tolerable limits (Leshchinsky 2009; Vahedifard *et al.* 2013). By using other design methods available for geosynthetic-reinforced slopes based on a displacement approach (Gourc *et al.* 1986; Lemonnier *et al.* 1998b, a) or based on in situ measurements (Allen *et al.* 2003; Bathurst *et al.* 2008; Tin *et al.* 2011), it is possible to estimate the failure limit state, verifying the serviceability limit state of a structure.

The displacement approach procedure considers an imposed displacement at the top of the slope (and therefore a related displacement at each layer) in order to mobilise tensions in the reinforcements. Displacement methods require load-displacement curves determined through the use of pullout tests. Intrinsically, these design procedures must take into account the analysis in terms of active length described in this paper.

5 CONCLUSIONS

Active length refers to the portion of a geogrid specimen on which the mobilization of interaction mechanisms, under pullout conditions, withstands the applied pullout load. In order to study the actual behaviour of the soil-geosynthetic interface, it is important to determine the active length experimentally through the use of pullout tests. This paper reports the results of pullout tests performed on two HDPE, mono-directional, extruded geogrids in compacted, uniform, medium sand.

The following conclusions are suggested:

1) During the *tensile load transfer phase*, average longitudinal strain (mobilized on the active length) is an increasing function of vertical effective pressure. The gradient of the average longitudinal strain recorded in the transfer phase of the pullout load is smaller than that recorded in the pullout phase. Once average longitudinal strain stops increasing (equal to reaching the peak pullout force), pullout failure occurs.
2) The equivalent uniform average shear stress, τ_{AL}, which is mobilized along the interface between the soil and the active length of the geogrid, increases with increasing vertical effective pressure. During the *tensile load transfer phase*, τ_{AL} decreases with increasing clamp displacement, despite the local increase in frictional and passive stresses along the geogrid. When the *pullout phase* starts, τ_{AL} changes its trend, increasing with increasing displacement. Once longitudinal strain stops increasing, pullout occurs and average shear stress rapidly decreases.
3) For small displacements, once the entire specimen length has been mobilized, the values of the apparent coefficient of friction $\mu_{S/GSY}^{AL}$ of the interface calculated using the active length

are obviously higher than those calculated using the specimen length. This analysis could be used in order to evaluate, for different specimen lengths, the design value of the apparent coefficient of friction of the interface related to the admissible mobilized displacement of the reinforcement in the *tensile force transfer phase*.

4) The stiffness value able to predict, for the applied pullout load, the integrated response of soil reinforcement interaction along the active length was defined as apparent pullout stiffness $J_a^{\sec}$. During the *tensile load transfer phase* $J_a^{\sec}$, defined in equation (5), rapidly increases with increasing average longitudinal strain, which has very small values (1-2% for GGR1; 2-3% for GGR2). Under the same vertical effective pressure, short reinforcements show a lower maximum value of apparent pullout stiffness than do the long specimens. During the *pullout phase*, $J_a^{\sec}$ decreases with increasing average longitudinal strain until reaching the in-air tensile stiffness (for the same strain level). When pullout failure occurs, a sudden decrease in $J_a^{\sec}$ is observed.

5) The peak value of apparent pullout stiffness decreases with increasing vertical effective pressure (from 2936 to 1706 kN/m for GGR1 and from 1363 to 985 kN/m for GGR2). Moreover, the peak value is mobilized for an average strain that increases with increasing vertical effective pressure (from 0.6 to 3.6% for GGR1, and from 1.2 to 4.4% for GGR2). Generally, the peak value of the apparent pullout stiffness is greater than the unconfined stiffness for the same level of strain. These results depend on the fact that, under confined conditions, due to interface interaction mechanisms, the tensile load varies along the specimen (contrary to the unconfined case).

345 **References**

346 Abramento, M. & J.Whittle, A. (1995) Experimental evaluation of pullout analyses for planar
347 reinforcements. *Journal of Geotechnical Engineering,* **21(6)**: 486-492.

348 Alagiyawanna, A.M.N., Sugimoto, M., Sato, S., Toyota, H. (2001) Influence of longitudinal and
349 trasverse members on geogrid pullout behavior during deformation. *Geotextiles and Geomembranes,*
350 **19(8)**: 483-507.

351 Allen, T.M., Bathurst, R.J., Holtz, R.D., Walters, D., Lee, W.F. (2003) A new working stress method
352 for prediction of reinforcement loads in geosynthetic walls. *Canadian Geotechnical Journal*, **40**: 976-
353 994.

354 Bathurst, R.J. & Ezzein, F.M. (2015) Geogrid and Soil Displacement Observations During Pullout Using
355 a Transparent Granular Soil. Geotechnical Testing Journal, **38(5)**: 1-13.

356 Bathurst, R.J., Miyata, Y., Nernheim, A., Allen, A.M. (2008) Refinement of K-stiffness Method for
357 geosynthetic reinforced soil walls. *Geosynthetics International*, **15(4)**: 269-295.

358 Calvarano, L.S., Gioffrè, D., Cardile, G., Moraci, N. (2014) A stress transfer model to predict the pullout
359 resistance of extruded geogrids embedded in compacted granular soils. *In proceending of the 10th*
360 *International Conference on Geosynthetics*, ICG 2014. Berlin, Germany, 21-24 September 2014, Code
361 110984.

362 Cardile, G., Calvarano, L.S., Gioffrè, D., Moraci, N. (2014) Experimental evaluation of the pullout
363 active length of different geogrids. *In proceending of the 10th International Conference on*
364 *Geosynthetics*, ICG 2014. Berlin, Germany, 21-25 September 2014, Code 110984.

365 Cazzuffi, D., Calvarano, L.S., Cardile, G., Moraci, N., Recalcati, P. (2011) European experience in
366 pullout tests: The influence of geogrid's geometry and structure on interface behaviour. *Geosynthetics,*
367 **29(5)**: 42- 51.

368 Cazzuffi, D, Cardile, G, Gioffrè, D (2014a) Geosynthetic Engineering and Vegetation Growth in Soil
369 Reinforcement Applications. *Transportation Infrastructure Geotechnology,* **1(3-4)**: 262-300.

Cazzuffi, D., Moraci, N., Calvarano, L.S., Cardile, G., Gioffrè, D., Recalcati, P. (2014) The influence of vertical effective stress and of geogrid length on interface behaviour under pullout conditions. *Geosynthetics,* **32(2)**: 40-50.

EN-ISO (2008) 10319: Geosynthetics wide-width tensile test. *International Organization for Standardization*, Ginevra.

Ezzein, F.M. & Bathurst, R.J. (2014) A new approach to evaluate soil-geosynthetic interaction using a novel pullout test apparatus and transparent granular soil. Geotextiles and Geomembranes, 42(3): 246-255.

Gourc, J.P., Ratel, A., Delmas, P. (1986) Design of fabric retaining walls: the displacement method. *In proceending of the 3rd International Conference on Geotextiles*. Vienna, Austria, 2289-294, 1067-1072.

Jacobs, F., Ziegled, M., Vollmert, L., Ehrenberg, H. (2014) Explicit design of geogrids with a nonlinear interface model. In proceending of the X International conference on Geosynthetics. Berlin, Germany, 25 September.

Kongkitkul, W., Chantachot, T., Tatsuoka, F. (2014) Simulation of geosynthetic load–strain–time behaviour by the non-linear three-component model. *Geosynthetics International* **21(4)**: 244-255.

Laba, J.T., Kennedy, J.B., Seymour, P.H. (1984) Reinforced earth retaining wall under vertical and horizontal strip loading. *Canadian Geotechnical Journal*, **21:** 407-418.

Lemonnier, P., Soubra, A.H., Kastner, R. (1998a) Variational displacement method for geosynthetically reinforced slope stability analysis II. Global stability. *Geotextiles and Geomembranes,* **16**: 27-44.

Lemonnier, P., Soubra, A.H., Kastner, R. (1998b) Variational displacement method for geosynthetically reinforced slope stability analysis: I. Local stability. *Geotextiles and Geomembranes*, **16**: 1-25.

Leshchinsky, D. (2009) On Global Equilibrium in Design of Geosynthetic Reinforced Walls. *Journal of Geotechnical and Geoenvironmental Engineering*, **135(3)**: 309-315.

Moraci, N. & Cardile, G. (2008) Pull-out behaviour of different geosynthetics embedded in granular soils. *In proceending of the 4th Asian Regional Conference on Geosynthetics*. Shanghai, China, 17÷20 June.

Moraci, N. & Cardile, G. (2009) Influence of cyclic tensile loading on pullout resistance of geogrids embedded in a compacted granular soil. *Geotextiles and Geomembranes*, **27**: 475-487.

Moraci, N. & Cardile, G. (2012) Deformative behaviour of different geogrids embedded in a granular soil under monotonic and cyclic pullout loads. *Geotextiles and Geomembranes*, **32**: 104-110.

Moraci, N., Cardile, G., Gioffrè, D. (2007) A theoretical method to predict the pullout behaviour of extruded geogrids embedded in granular soils. In proceending of the 5th International Symposium on Earth Reinforcement. Fukuoka, Japan, 14÷16 November.

Moraci, N., Cardile, G., Gioffrè, D., Mandaglio, M.C., Calvarano, L.S., Carbone, L. (2014a) Soil Geosynthetic Interaction: Design Parameters from Experimental and Theoretical Analysis. *Transportation Infrastructure Geotechnology*, **1(2)**: 165-227.

Moraci, N., Cazzuffi, D., Calvarano, L.S., Cardile, G., Gioffrè, D., Recalcati, P. (2014b) The influence of soil type on interface behavior under pullout conditions. *Geosynthetics*, **32(3)**: 42-50.

Moraci, N. & Gioffrè, D. (2006) A simple method to evaluate the pullout resistance of extruded geogrids embedded in a compacted granular soil. Geotextiles and Geomembranes, **24(3)**: 198-199.

Moraci, N, Mandaglio, MC, Gioffrè, D, Cardile, G, Cazzuffi, D, Recalcati, P, Starrantino, C (2009) Temperature monitoring of a geosynthetic-reinforced embankment in a seismic area. *In proceending of the 17th International Conference on Soil Mechanics and Geotechnical Engineering, ICSMGE 2009*. Code 92003.

Moraci, N. & Recalcati, P. (2006) Factors affecting the pullout behaviour of extruded geogrids embedded in compacted granular soil. *Geotextiles and Geomembranes*, **24(4)**: 220-242.

Ochiai, H., Hayashi, S., Otani, J., Hirai, T. (1992) Evaluation of pull-out resistance of geogrid reinforced soils. *In proceending of the International Symposium on Earth Reinforcement Practice*. Fukuoka, Japan, 141-146.

Palmeira, E.M. (2009) Soil–geosynthetic interaction: Modelling and analysis. Geotextiles and Geomembranes, 27368-390.

Perkins, S.W. & Cuelho, E.V. (1999) Soil-geosynthetic interface strength and stiffness relationships from pullout tests. *Geosynthetics International*, **6(5)**: 321-346.

Sugimoto, M., Alagiyawanna, A.M.N., Kadoguchi, K. (2001) Influence of rigid and flexible face on geogrid pullout tests. *Geotextiles and Geomembranes*, **19(5)**: 257-277.

Tin, N., Bergado, D.T., Voottipruex, P., Tanchaisawat, T. (2011) Modification of K-stiffness method for MSE structures on soft ground. *Geosynthetics International*, **18(5)**: 304-321.

Vahedifard, F., Leshchinsky, D., Meehan, C.L. (2013) Displacement-based internal design of geosynthetic-reinforced earth structures subjected to seismic loading conditions. *Geotechnique*, **63(6)**: 451-462.

Vieira, C.S., Lopes, M.d.L., Caldeira, L.M. (2013) Sand-geotextile interface characterisation through monotonic and cyclic direct shear tests. *Geosynthetics International*, **20(1)**: 26-38.

Wang, Z., Jacobs, F., Ziegler, M. (2014) Visualization of load transfer behaviour between geogrid and sand using PFC2D. *Geotextiles and Geomembranes*, **42(2)**: 83-90.

Zhou, J., Chen, J.-F., Xue, J.-F., Wang, J.-Q. (2012) Micro-mechanism of the interaction between sand and geogrid transverse ribs. Geosynthetics International, **19(6)**: 426-437.

Ziegler, M. & Timmers, V. (2004) A new approach to design geogrid reinforcement. In proceending of the 3rd European Geosynthetics Conference. Munich, Germany, 01-03 March.

439

List of notation

σ_V'	Vertical effective pressure (kPa)
B_R	Node thickness (mm)
B_T	Thickness of the bar portion between two nodes (mm)
δ	Clamp displacement (mm)
ΔL	Elongation (mm)
D_{10}	Grain size corresponding to 10% in weight of passing soil (mm)
D_{50}	Average grain size (mm)
D_{60}	Grain size corresponding to 60% in weight of passing soil (mm)
ε_{AP}	Average longitudinal strain calculated at the beginning of the pullout phase (%)
ε_P	Tensile strain evaluated at T_P (at v=1 mm/min) (%)
ε_f	Tensile strain evaluated at tensile rupture (at v=1 mm/min) (%)
GGR1	Extruded Geogrid One
GGR2	Extruded Geogrid Two
$J_{2\%}$	Tensile stiffness at 2% of strain (kN/m)
$J_{5\%}$	Tensile stiffness at 5% of strain (kN/m)
J_a^{sec}	Apparent pullout stiffness (kN/m)
L_A	Active length (mm)
L_R	Specimen length (mm)
L_T	Distance between two longitudinal ribs (mm)
P	Pullout load (kN/m)
P_{in}	Pullout trigger force (kN/m)
P_R	Pullout resistance (kN/m)
RVDT	Rotational Variable Displacement Transducer
S	Spacing between geogrid bearing members (mm)
τ_{AL}	Average shear-stress (kN/m^2)
T_n	Nominal tensile strength (kN/m)
T_P	Peak tensile strength at 1 mm/min displacement rate (kN/m)
U	Uniformity coefficient of soil (dimensionless)
v	Rate of displacement (mm/min)
S	Spacing between geogrid bearing members (mm)
w_{opt}	Optimum water content (%)
W	Pullout box width (mm)
W_B	Width of the bar (mm)
W_T	Width of the bar portion between two nodes (mm)
W_R	Node width (mm)

ϕ'	Soil shear strength angle (°)
ϕ'_{cv}	Soil shear strength angle at constant volume (°)
ϕ'_{p}	Peak shear strength angle (°)
γ_{dmax}	Maximum dry unit weight (kN/m^3)
$\mu_{S/GSY}$	Soil-geosynthetic peak interface apparent coefficient of friction (dimensionless)
$\mu^{AL}_{S/GSY}$	Soil-geosynthetic peak interface calculated using L_A (dimensionless)

441 **Tables**

442 *Table 1. Structural and the mechanical properties of the geogrids used in the research.*

Geogrid	GGR1 - Mono-directional extruded HDPE	GGR2 -Mono-directional extruded HDPE
T_n [kN/m]	120.00	60.00
T_P [kN/m]	98.93	49.28
ε_P [%]	13.7	13.9
ε_f [%]	17.8	20.2
$J_{2\%}$ [kN/m]	1749	865
$J_{5\%}$ [kN/m]	1211	613
S [mm]	220	220
W_T [mm]	4.2	8.5
B_T [mm]	4.9	2.9
W_R [mm]	14.1	13.0
B_R [mm]	6.8	4.6
W_B [mm]	17.3	10.5

443

444

445 *Table 2. Average longitudinal strain calculated at the beginning of the pullout phase (ε_{AP}) for each*
446 *specimen length and vertical effective pressure.*

Geogrid	σ'_v [kPa]	$\varepsilon_{AP-0.4}$ [%]	$\varepsilon_{AP-0.9}$ [%]	$\varepsilon_{AP-1.15}$ [%]
GGR1	10	0.7	0.6	0.6
GGR1	25	0.8	1.1	1.4
GGR1	50	0.8	1.8	2.6
GGR1	100	2.1	3.4	4.8
GGR2	10	1.0	1.2	1.2
GGR2	25	1.3	1.8	2.5
GGR2	50	2.5	3.0	4.5
GGR2	100	3.2	5.2	5.6

447

448

449 *Table 3. Influence of vertical effective pressure on the peak value of the apparent pullout stiffness of the*
450 *GGR1 for the same specimen length (L_R = 1.15 m)*

σ'_V [kPa]	J_A max [kN/m]	ε_A [%]	J in-air [kN/m]	J_A max /J in-air [-]
10	2936	0.56	2229	1.32
25	2645	1.38	1857	1.42
50	2331	1.73	1789	1.30
100	1706	3.62	1394	1.22

451

Table 4. Influence of vertical effective pressure on the peak value of the apparent pullout stiffness of the GGR2 for the same specimen length (L_R = 1.15 m)

σ'_V [kPa]	J_A max [kN/m]	ε_A [%]	J in-air [kN/m]	J_A max /J in-air [-]
10	1363	1.20	1101	1.24
25	1223	2.28	844	1.45
50	1058	3.25	737	1.44
100	985	4.36	656	1.50

Figures

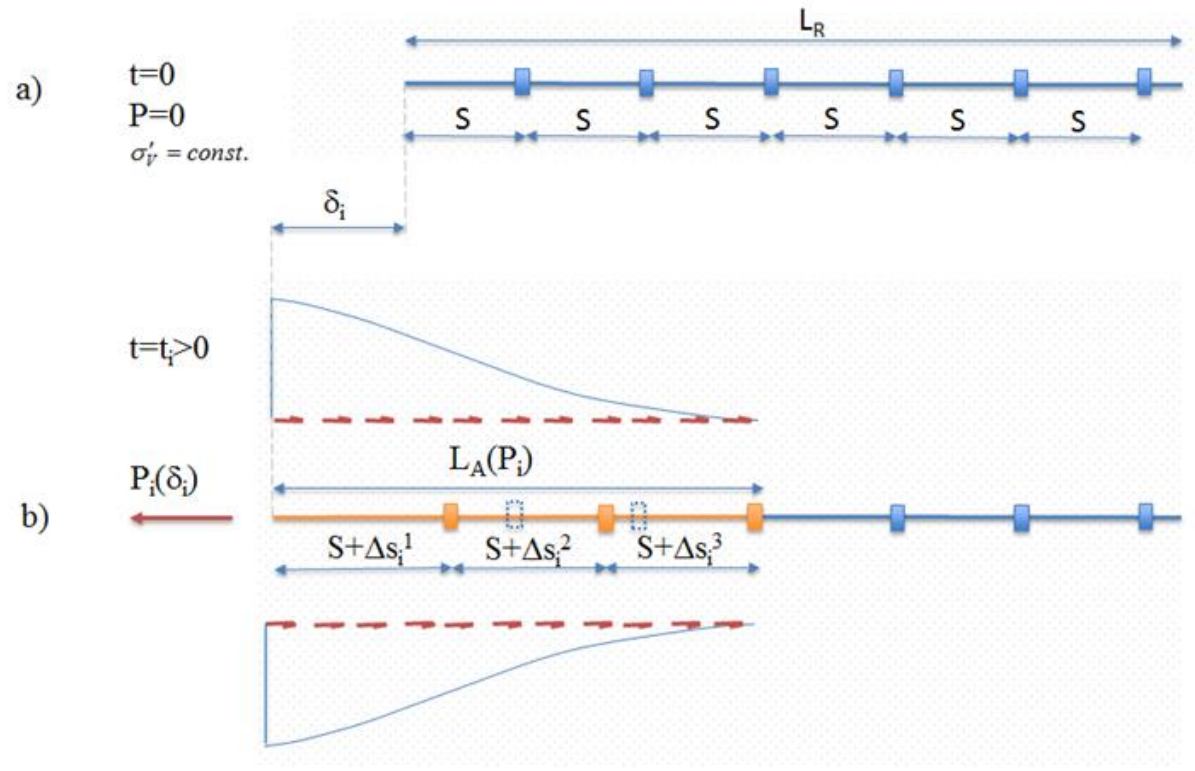

Figure 1. Pullout load transfer mechanism; (a) P=0 (b) P>0

459

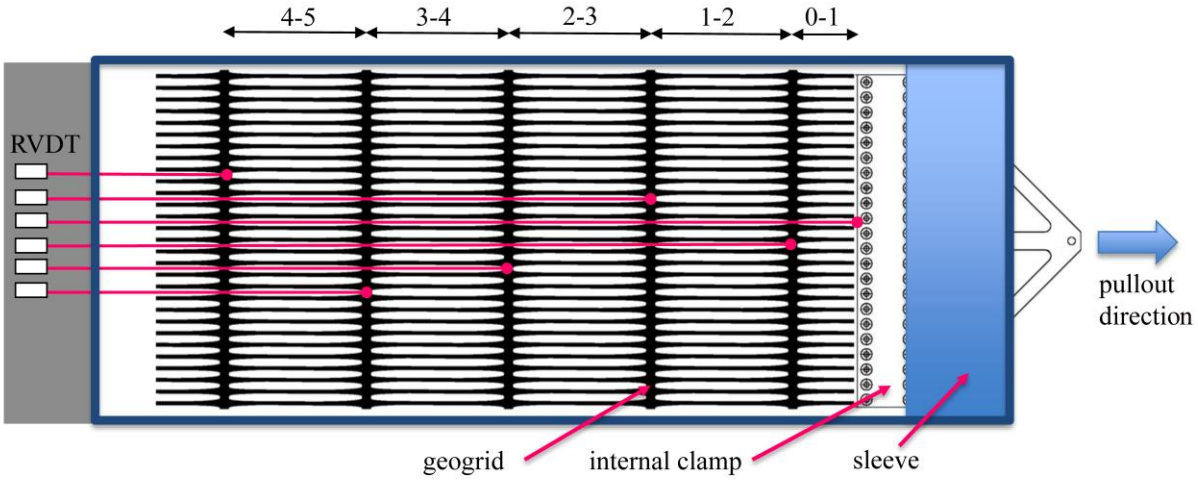

460

461 *Figure 2. System to measure displacement along the specimen length.*

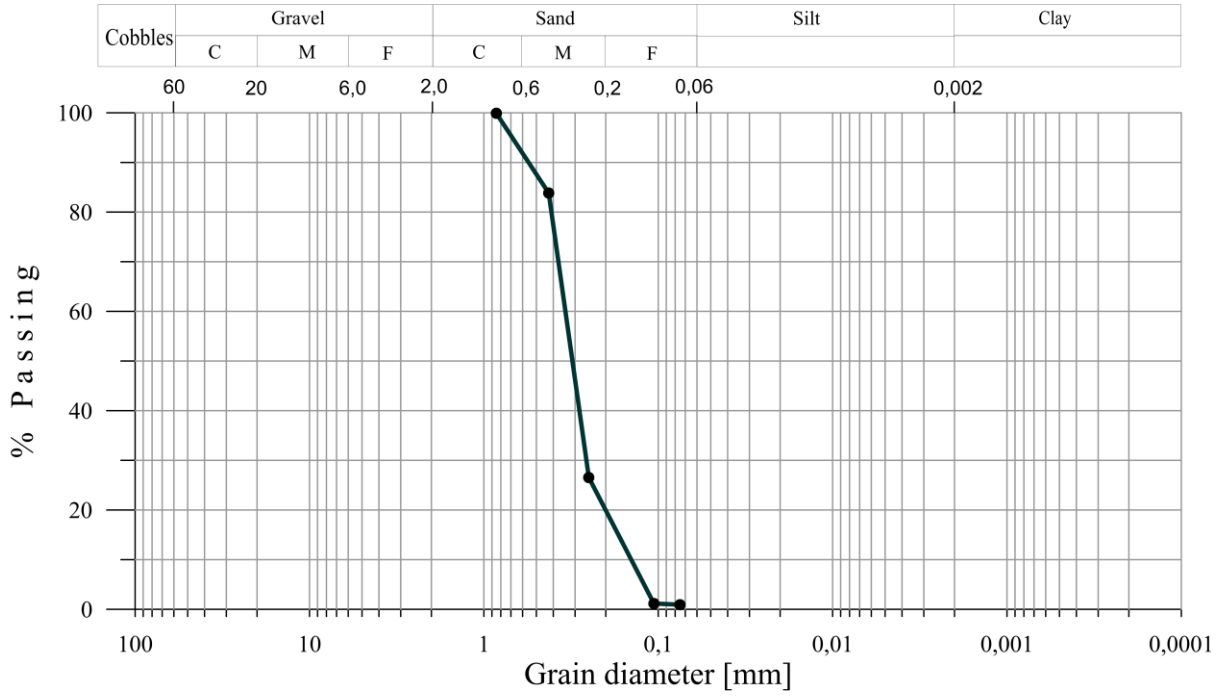

Figure 3. Soil grain size distribution curve.

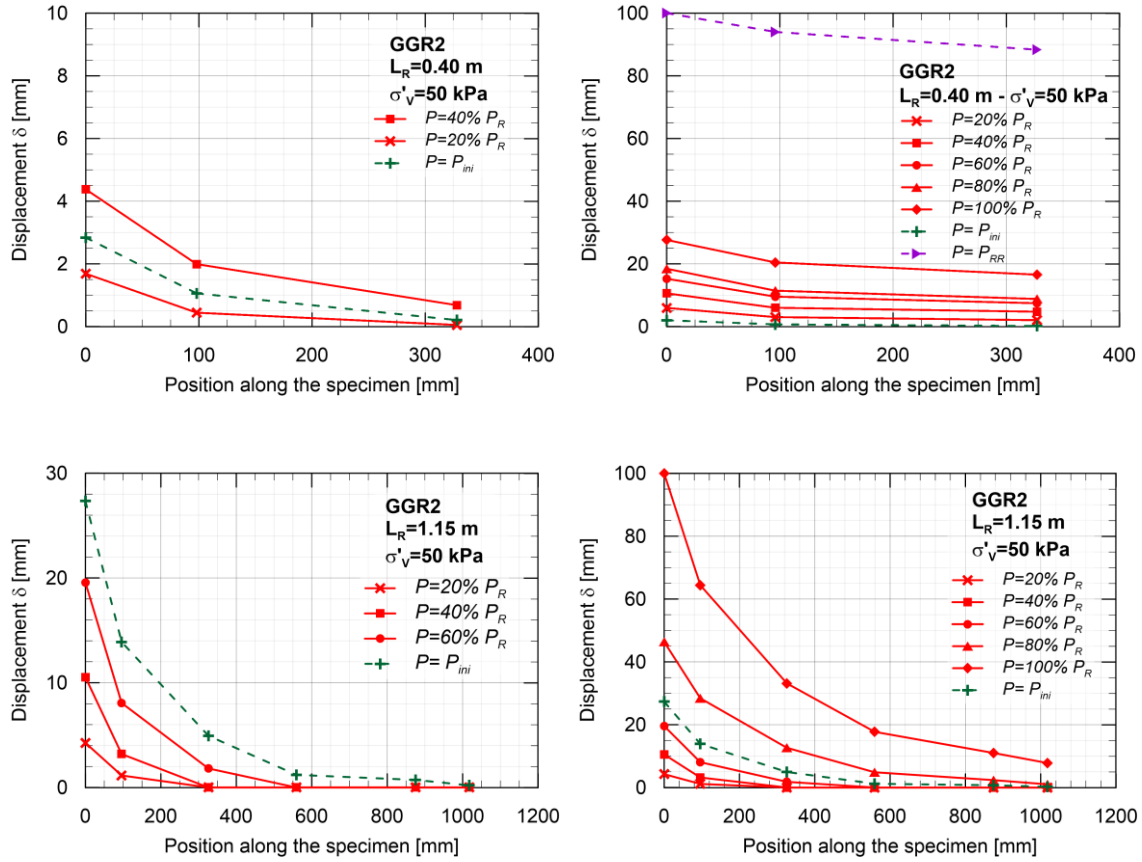

(a) (b)

Figure 4. Distributions of the nodal displacements along the geogrid specimen GGR2 for a fixed vertical effective pressure (50 kPa) and for different values of the applied pullout force. The upper graphs refer to short reinforcement, while the lower graphs refer to long reinforcement, showing both the tensile load transfer phase (a) and the pullout phase (b).

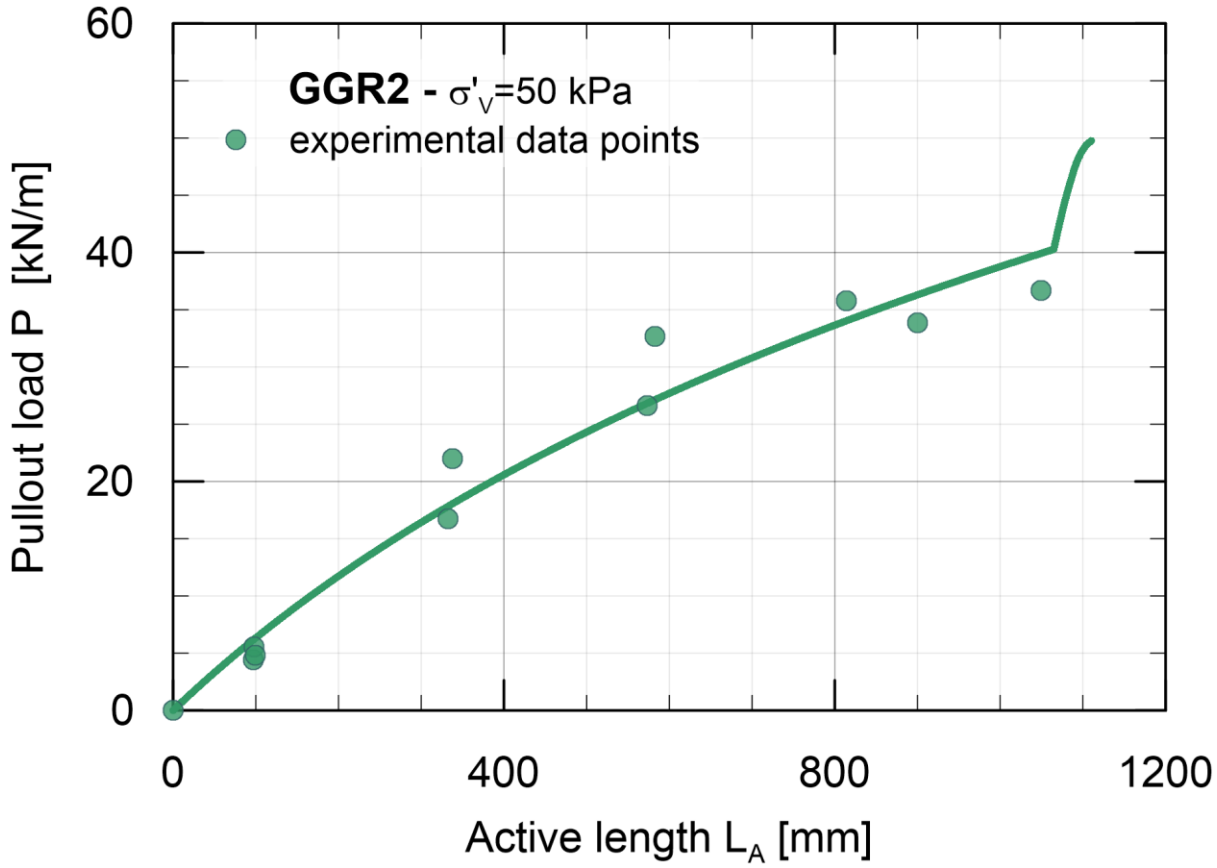

Figure 5. Experimental evaluation of the active length for the geogrid GGR2 at fixed vertical effective pressure (50 kPa).

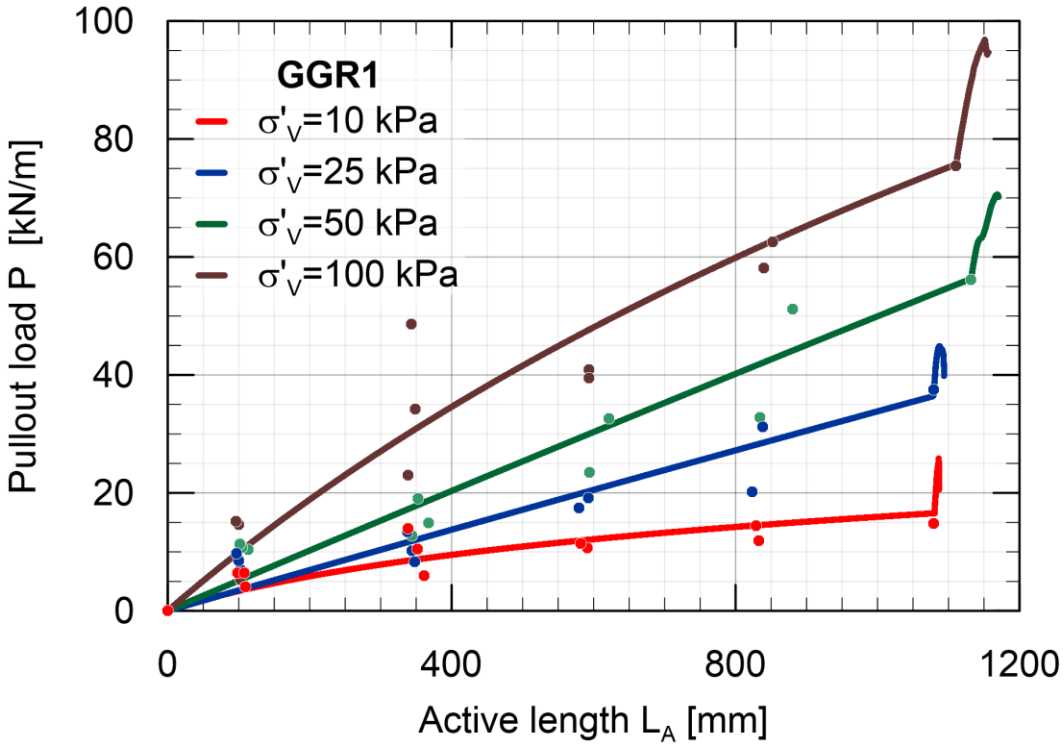

(a)

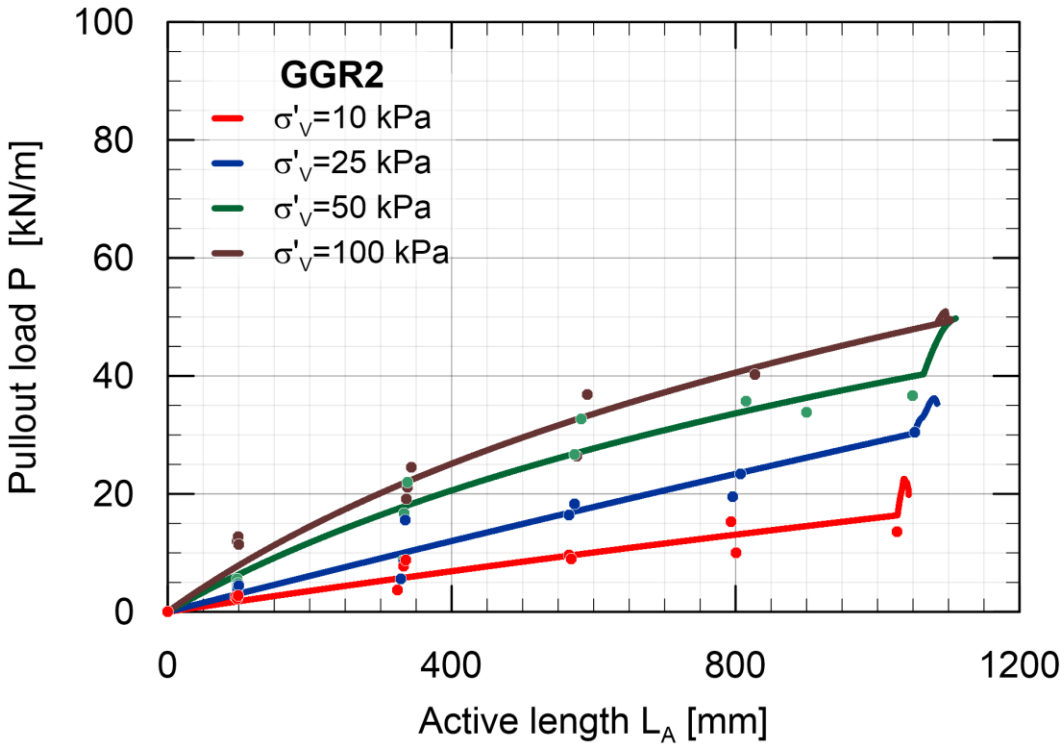

(b)

Figure 6. Active length versus pullout load obtained for the GGR1 (a) and GGR2 (b) geogrids, varying the vertical effective pressure.

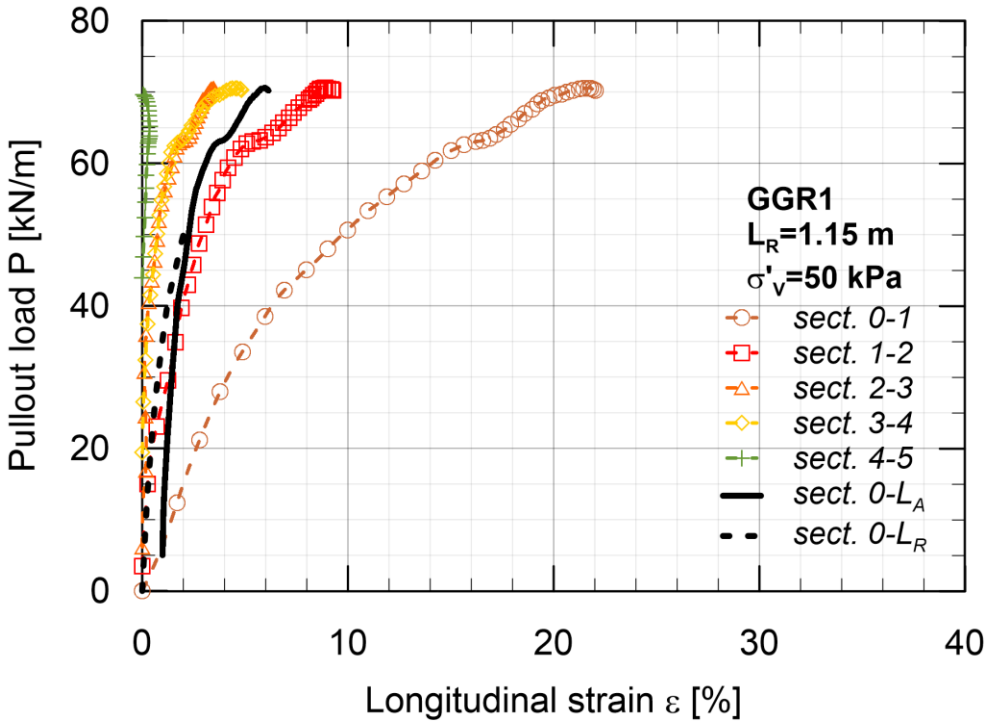

(a)

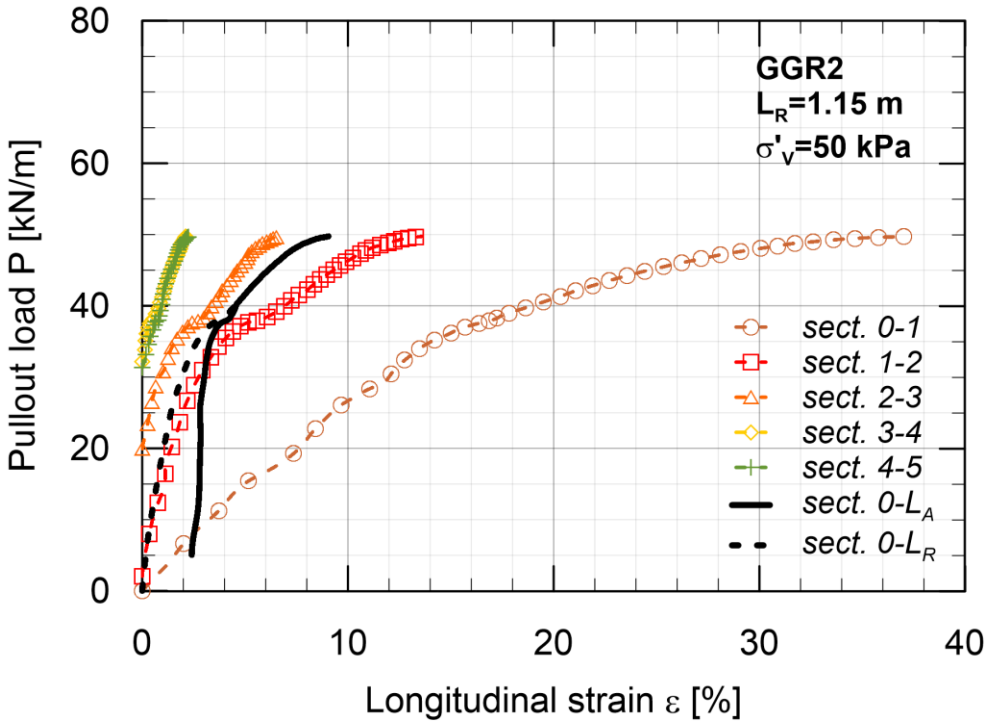

(b)

Figure 7. Longitudinal strain related to the different portions of the geogrid versus pullout load, (a) GGR1 and (b) GGR2.

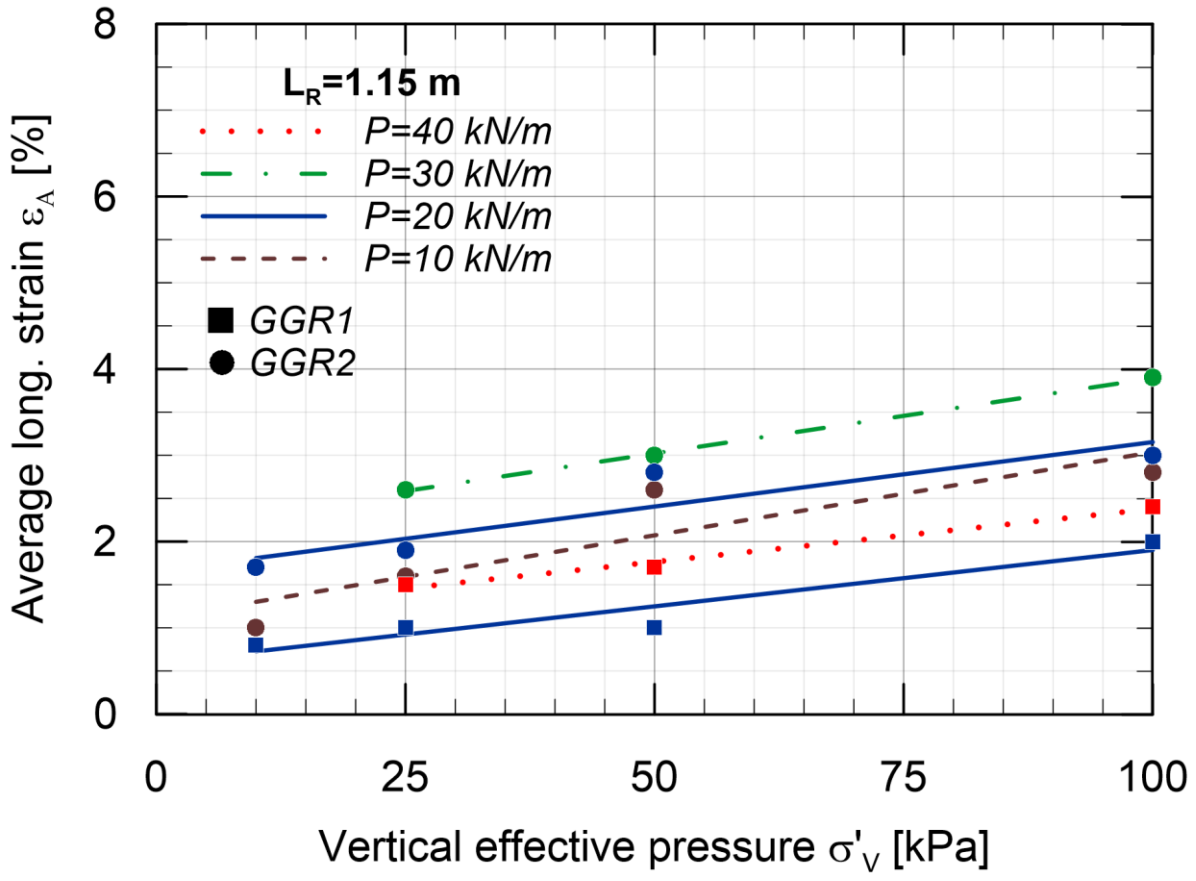

Figure 8. Influence of vertical effective pressure on the average strain mobilized on the active portion of the geogrid specimen (0-L_A) under different pullout loads (iso-pullout load curves) during the tensile load transfer phase.

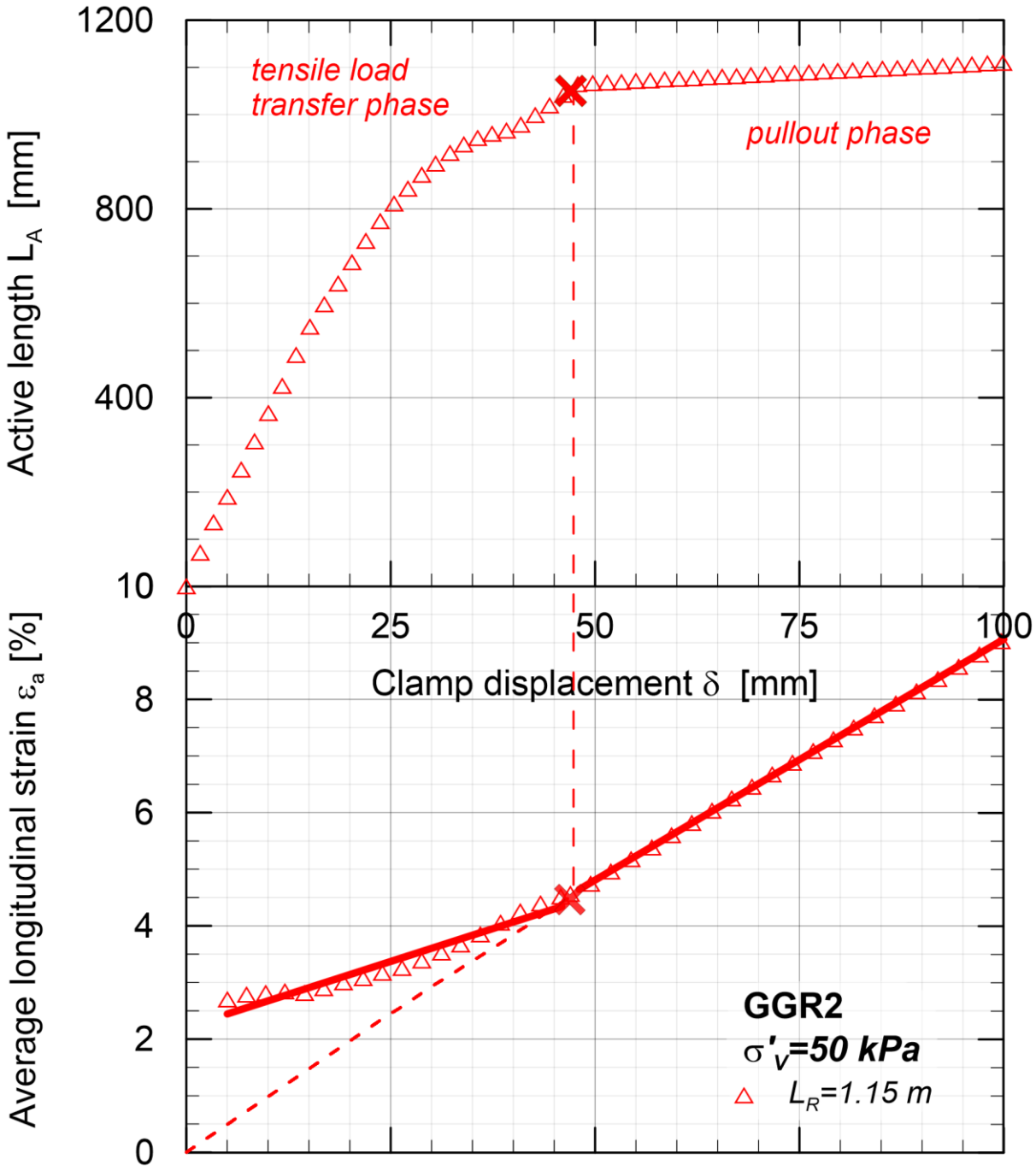

Figure 9. Clamp displacements versus active length (upper graph) and versus average longitudinal strain (lower graph) calculated for the GGR2 geogrid under a vertical effective pressure of 50 kPa and for a specimen length L_R=1.15 m.

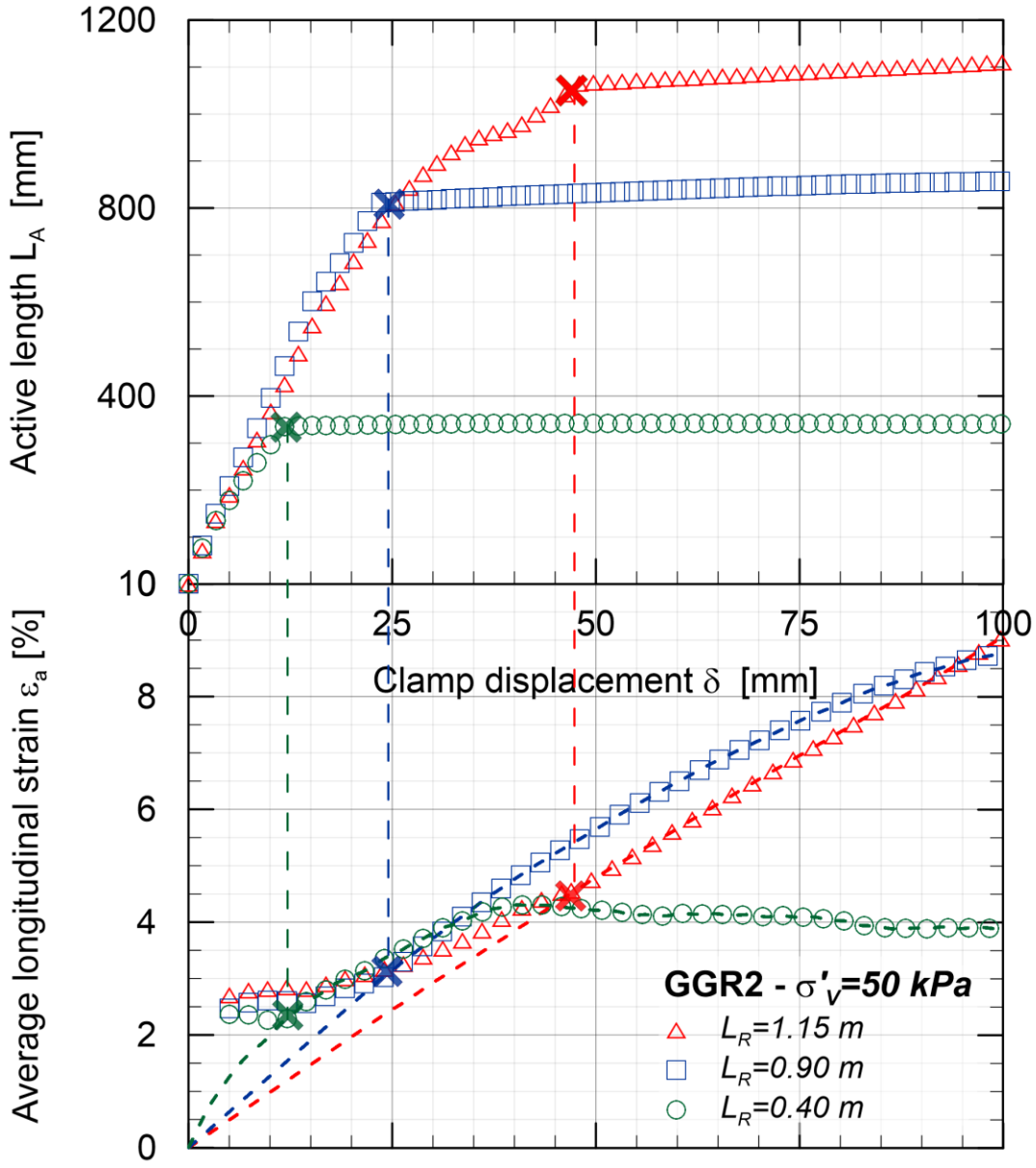

Figure 10. Clamp displacements versus active length (upper graph) and versus average longitudinal strain (lower graph) calculated for the GGR2 geogrid under a vertical effective pressure of 50 kPa and varying the specimen length.

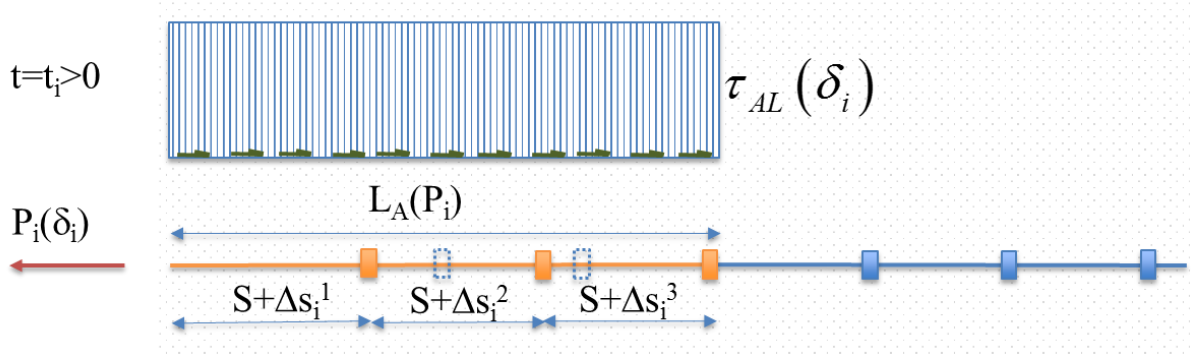

510

511 *Figure 11. Equivalent, uniform shear-stress distribution.*

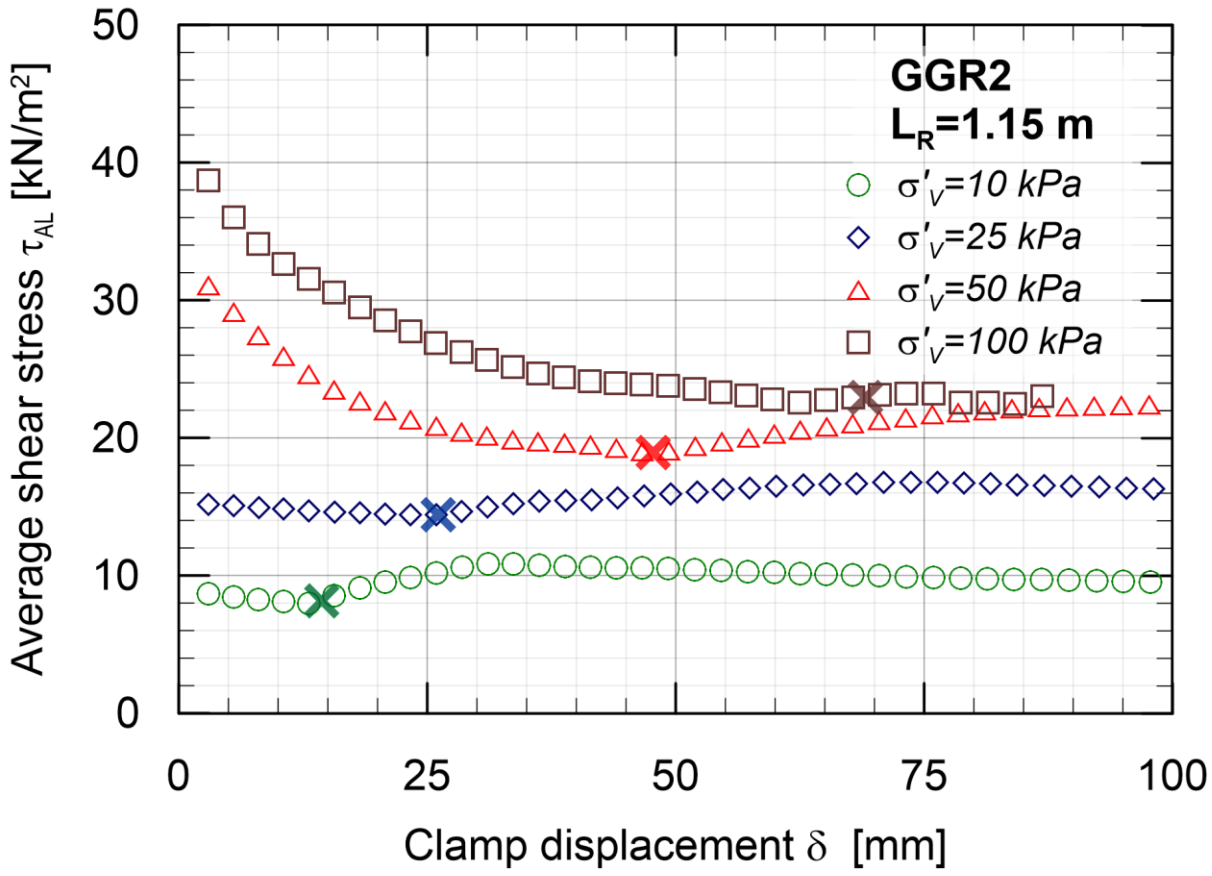

Figure 12. Average shear stress (equivalent, uniform shear-stress distribution) versus clamp displacement calculated for the GGR2 of length equal to 1.15 m and varying the vertical effective pressure.

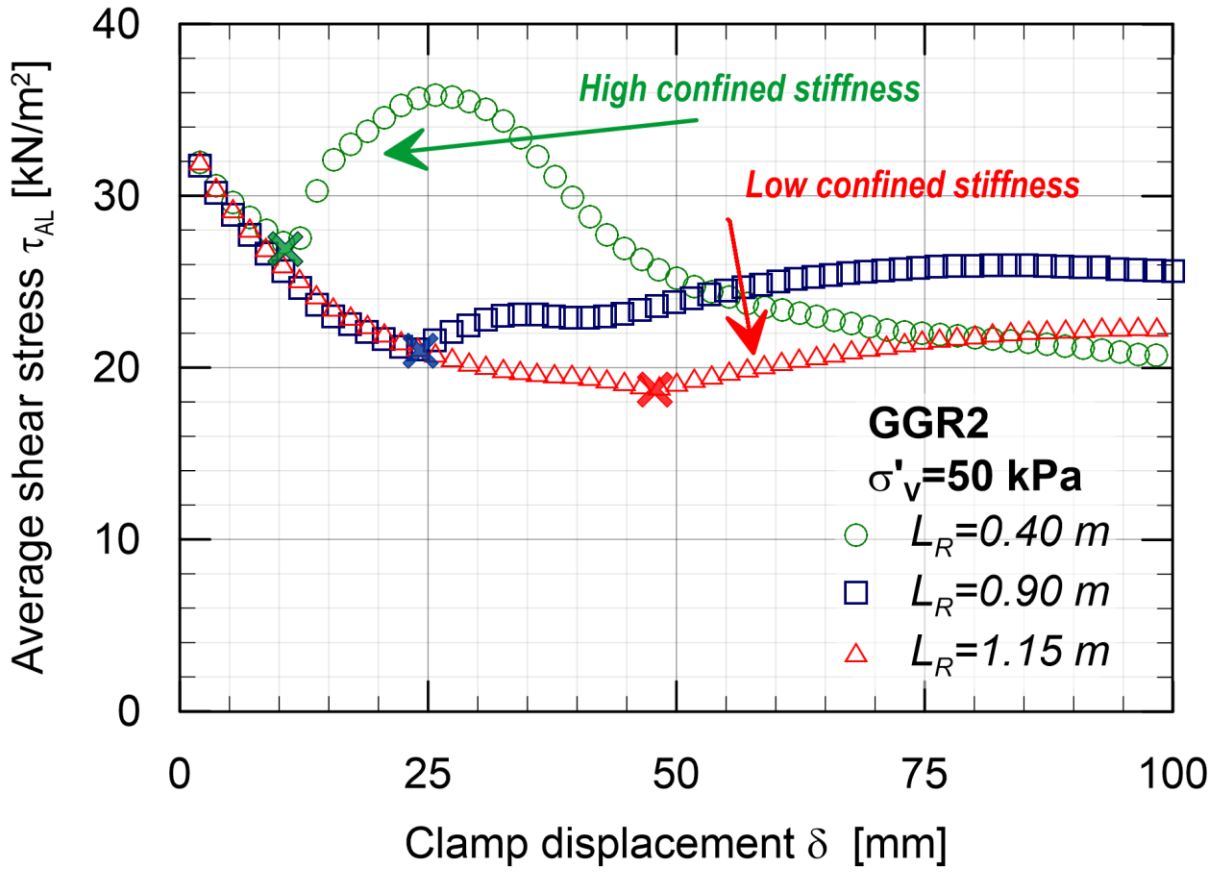

Figure 13. Pullout behaviour in terms of average shear stress (equivalent, uniform shear-stress distribution) of the geogrid GGR2 for a fixed vertical effective pressure (50 kPa) and varying the specimen lengths.

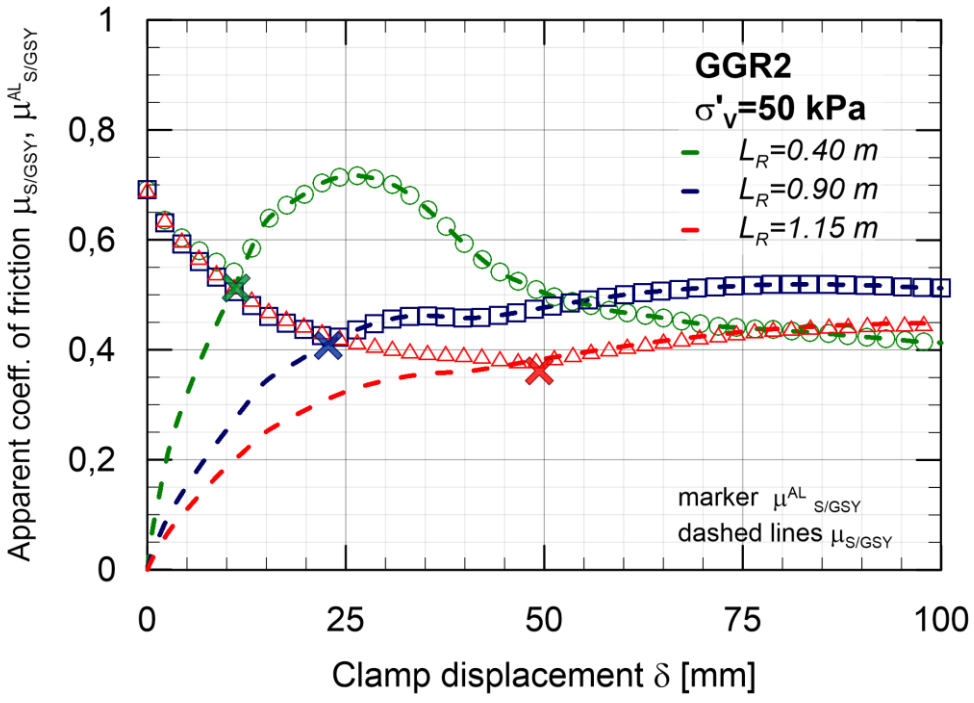

(a)

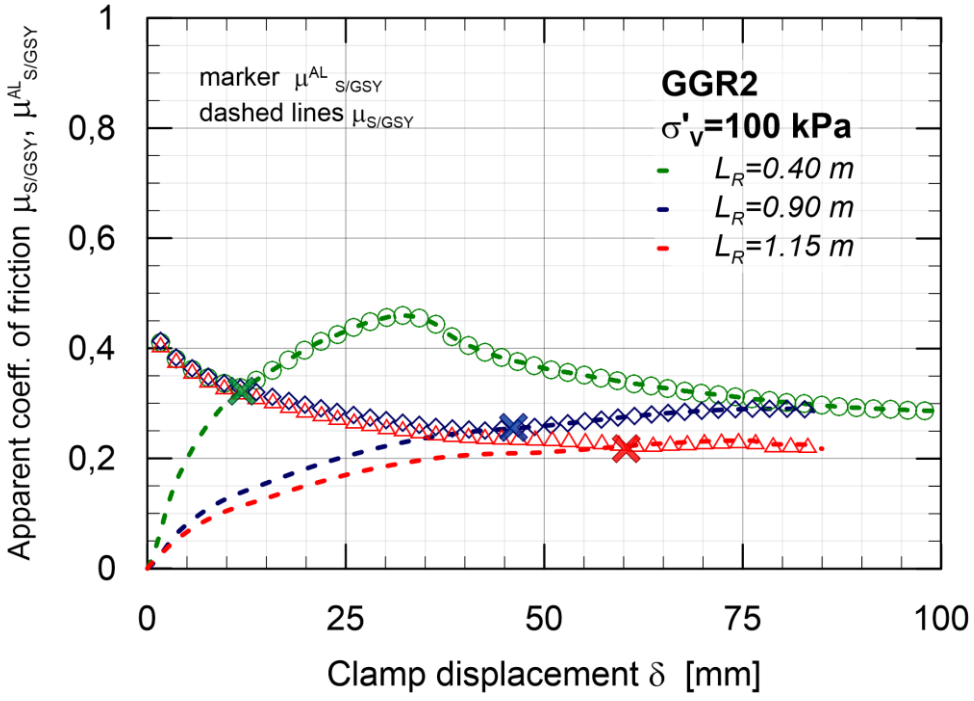

(b)

Figure 14. Apparent coefficient of friction of the soil-geosynthetic interface versus clamp displacement calculated for the GGR2 geogrid under vertical effective pressures of 50 kPa (a) and 100 kPa (b) and varying the specimen length.

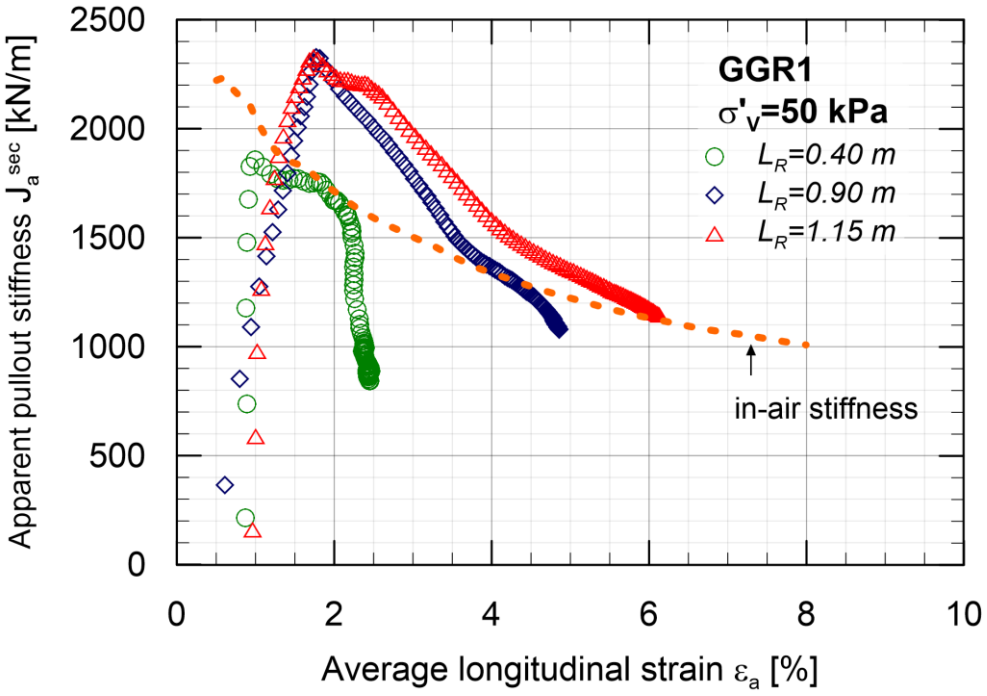

(a)

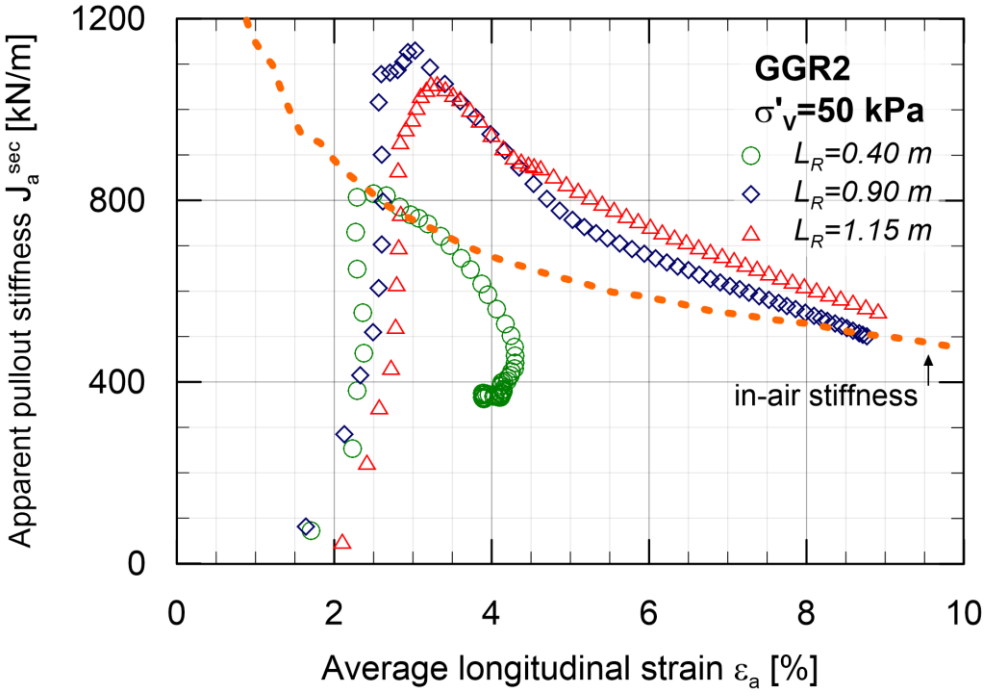

(b)

Figure 15. Apparent pullout stiffness versus average longitudinal strain obtained by pullout test performed on GGR1 (a) and GGR2 (b) geogrid of different specimen lengths and under the same vertical effective pressure (50 kPa).

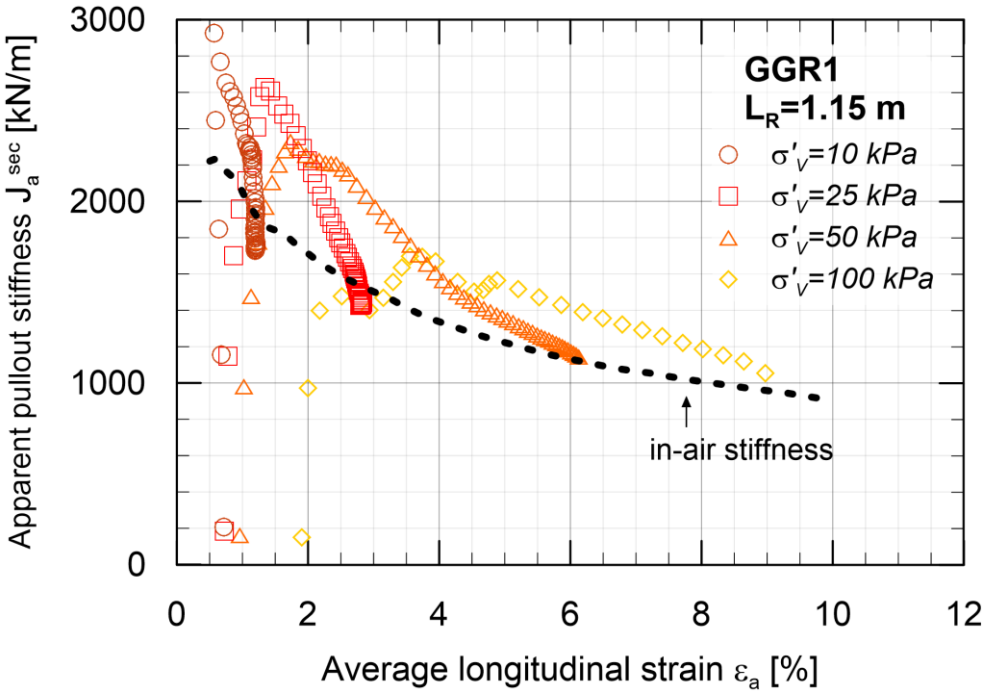

(a)

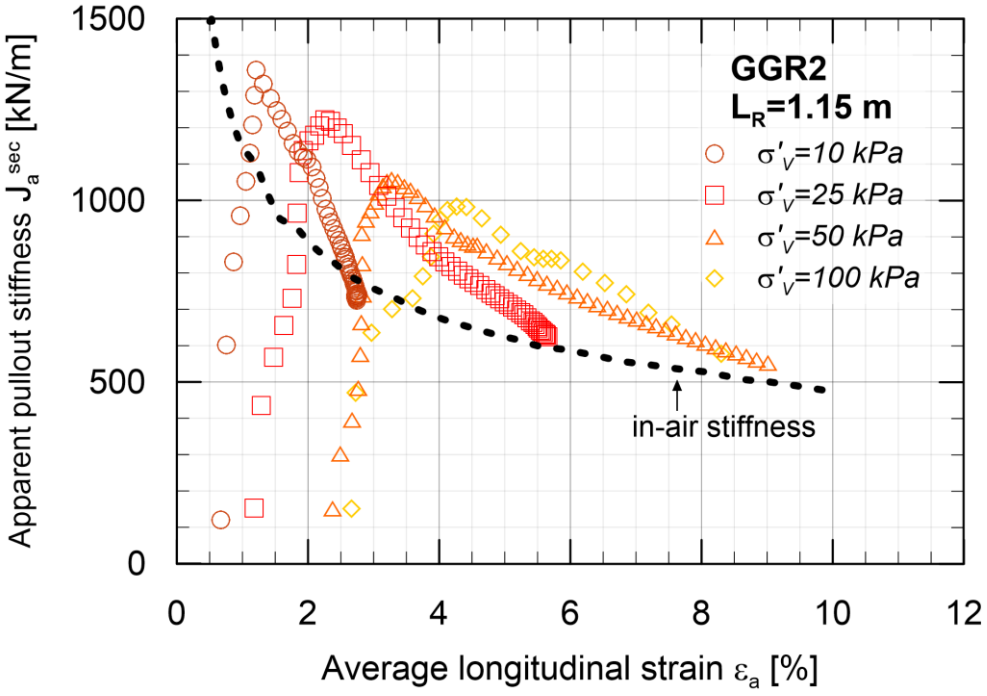

(b)

Figure 16. Influence of vertical effective pressure on the apparent pullout stiffness for GGR1 (a) and GGR2 (b) geogrid of specimens length L_R= 1.15 m.

548

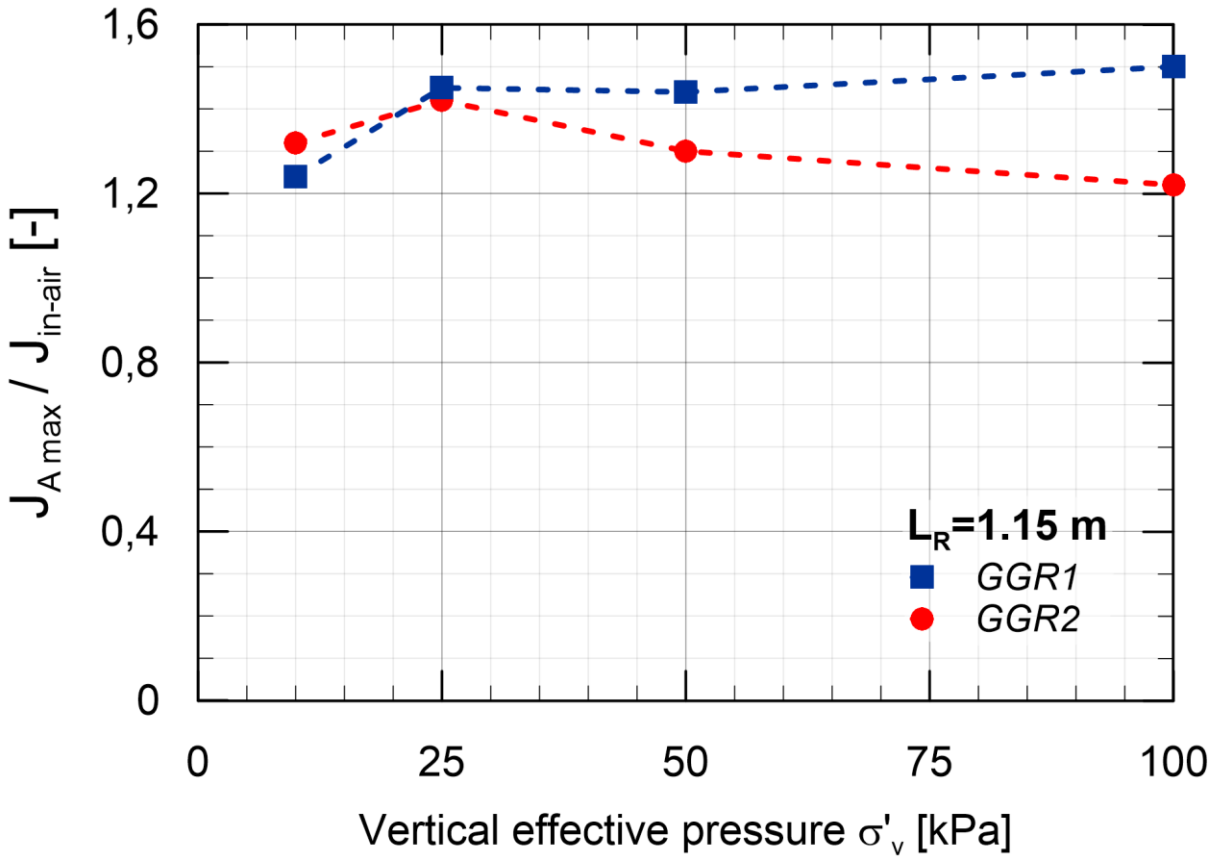

549

550 *Figure 17. Ratio between pullout confined stiffness and in-air stiffness versus vertical effective pressure*

551 *obtained for different geogrids of L_R=1.15 m.*

552